An Optimal Energy Management Technique Using the ϵ-Constraint Method for Grid-Tied and Stand-Alone Battery-Based Microgrids

ELIAN J. AGNOLETTO[ID][1]**, DANIEL SILVA DE CASTRO**[ID][1]**, RODOLPHO V. A. NEVES**[ID][2]**,
RICARDO QUADROS MACHADO**[ID][1]**, (Senior Member, IEEE), AND
VILMA A. OLIVEIRA**[ID][1]**, (Member, IEEE)**

[1]São Carlos School of Engineering, University of São Paulo, São Carlos 13566-590, Brazil
[2]Department of Electrical Engineering, Federal University of Viçosa, Viçosa 36570-900, Brazil

Corresponding author: Elian J. Agnoletto (elianmt@usp.br)

ABSTRACT The intermittent characteristics of microgrids (MGs) have motivated the development of energy management systems (EMSs) in order to optimize the use of distributed energy resources. In current studies, the implementation of an EMS followed by experimental-based analyses for both grid-tied and stand-alone MG operation modes is often neglected. Additionally, the design of a management strategy that is capable of preserving the storage device lifetime in battery-based MGs using a power gradient approach is hardly seen in the literature. In this context, this work presents the application of an EMS for battery-based MGs which is suitable for both grid-tied and stand-alone operation modes. The proposed EMS is formulated as an optimal power flow (OPF) problem using the ϵ-constraint method which is responsible for computing the current references used by the EMS to control the MG sources. In the optimization problem, the total generation cost is minimized such that the active power losses are kept within pre-established boundaries, and a battery management strategy based on power gradient limitation is included. Finally, the effectiveness of the proposed EMS is evaluated by two scenarios which enable detailed analyses and validation. The first considers a dispatchable and a non-dispatchable source, whereas the second a dispatchable source and a storage device. The experimental results showed that the proposed EMS is efficient in both operation modes and is also capable of smoothing the state of charge (SoC) behavior of the storage device.

INDEX TERMS Battery power gradient, distributed generation, energy management system, microgrid, optimal power flow, storage device.

I. INTRODUCTION

The connection of distributed generators (DGs) to electrical power systems and the renewable energy sources intermittent characteristics have motivated the study of energy management strategies to optimize microgrids (MGs) operations, therefore improving DGs performance in an intelligent, safe, reliable and coordinated way [1].

The control concepts applied to MGs are established hierarchically through the primary, secondary and tertiary levels. The energy management is executed at the tertiary level by

The associate editor coordinating the review of this manuscript and approving it for publication was Zhen Li.

solving an optimal power flow (OPF) problem which optimizes the energy resources usage [2]. This is performed based on an objective function differentiation. Typically, the OPF considers power balance constraints, emission of pollutants, fuel cost, performance, security boundaries, power sharing and stability [1], [3]–[9].

Basically, an energy management system (EMS) is addressed following either a decentralized or a centralized architecture. In the former, the management strategy runs locally with slow communication links. In the latter, on the other hand, it operates on the highest control layer and fast communication links are required [10]. The advantage of the centralized approach is that the EMS configuration provides

broad observability of the MGs, which promotes optimal overall operation in terms of voltage and current (amplitude and phase) minimal requirements to run an optimization algorithm which computes each operating point that will be sent to the DGs.

In terms of MGs applications, it is important to state that although the centralized approach incorporates the aforementioned advantages, the data communication link between the control unit and the management unit must be implemented in a way to avoid unnecessary power consumption and data congestion, leading to low efficiency and additional delays, thus compromising the EMS performance. Depending on the amount of data demanded by the management unit and the MG size, the event trigger or data-driven strategy for data processing and communication can be suitably used to reduce or overcome these issues [11], [12].

Unfortunately, there are conditions where the centralized EMS algorithm does not consider connection impedances among sources, in which case the equality constraints are solely described by the power balance at the point of common coupling (PCC) [13]–[16]. However, when impedances are considered, the equality constraints are given by power flow equations and the MG buses voltage constraints can be introduced into the OPF formulation [6], [9], [17]. In this way, the optimization algorithm is capable of finding solutions in which the voltages are kept within the limits established according to power quality standards.

In general, the OPF problem optimizes multi-objective functions using heuristic-based methods, such as genetic algorithm, ant colony and particle swarm, or even classical methods as weighted sum and ϵ-constraint [6], [7], [9], [16], [18]–[20]. The heuristic-based methods are procedures in which the gradient information is not used into the searching process [18]. Although these methods find feasible solutions for the objective function, they do not ensure optimality [21].

Some proposed algorithms solve the OPF problem by using the weighted sum method that assigns weights for the objectives and transforms the multi-objective searching into a mono-objective problem [9]. Even though weighted sum methods are intuitive and easy to approach, it does not find the optimal Pareto's solutions when the problem is non-convex, which is the case of the OPF [18]. In addition, the normalization and the weights assigned to each function have to be performed accurately, since it is important that the weights express the different objectives real effect [18]. The ϵ-constraint method is an alternative solution to reduce the difficulties of the weighted sum when solving non-convex problems. This method optimizes one objective and considers the others as inequality constraints [18].

The MGs operate in grid-tied and stand-alone modes. Nevertheless, in the majority of papers only one of them is evaluated, where the droop controller technique is usually employed to ensure power sharing among the DGs and the main grid [4], [9], [14], [22], [23]. However, its disadvantage appears when the MG is in stand-alone mode, where a secondary control loop is required to correct the

steady-state voltage and frequency deviations caused by the droop controllers.

Alternatively, a switching control strategy can be used as another technique to keep MGs in proper operation. In this case, the operation in the grid-tied mode is performed by regulating the DGs output currents injected into the grid, whereas in the stand-alone mode the voltage and frequency regulations are performed according to a master DG with slave DGs operating in current control mode [16]. This approach is addressed in [16], [24] and [25]. However, the power flow equations and battery power gradient are not considered as constraints, what leads to an untied bus voltage and battery lifetime degradation, respectively.

As for batteries, the power gradient, the large state of charge (*SoC*) variations (>50%), the charging and discharging cycles and the idle-time are commonly responsible to speed-up the battery degradation [8], [26]–[28]. An effective solution for saving the device lifetime, which is usually approached in the literature, is based on the battery power gradient limitation introduced in the objective function or in the optimization problem constraints [8], [17]. In [17], a quadratic term was inserted into the objective function to penalize high rates of power variation in the storage devices. Nevertheless, this type of procedure underuses the battery power delivery capability and thus increases operational costs. In order to overcome this drawback, an inequality constraint that limits the power gradient can be included in the OPF problem formulation [8]. However, this constraint alone does not ensure the optimization algorithm convergence along all the operating points, specifically when the *SoC* reaches its minimum or maximum thresholds.

This work proposes an optimal centralized EMS for grid-tied and stand-alone MGs composed by dispatchable and non-dispatchable sources, as well as energy storage devices. In a way to reduce the weighted sum method implementation difficulties, which are related to the weights definition and the objectives normalization values, the EMS optimization algorithm is based on the solution of an OPF problem performed according to the ϵ-constraint method. This algorithm minimizes the MG total generating cost and keeps the active power losses below a pre-established value. Since batteries are expensive devices in MGs, an additional power gradient constraint which is set to prevent its degradation and thus preserve their lifetime was introduced in the optimization problem formulation. Experimental tests were carried out to evaluate the proposed EMS in terms of MG energy management and effectiveness in reducing battery degradation by avoiding high battery power and *SoC* gradients.

II. SYSTEM DESCRIPTION

The MG studied in this work is composed by two three-phase voltage source inverters (VSIs). These VSIs are connected to the main grid through LCL filters, leading to the three buses shown in Fig. 1.

The buses 1, 2 and 3 correspond to the connection point of the two capacitors and the PCC, respectively. The
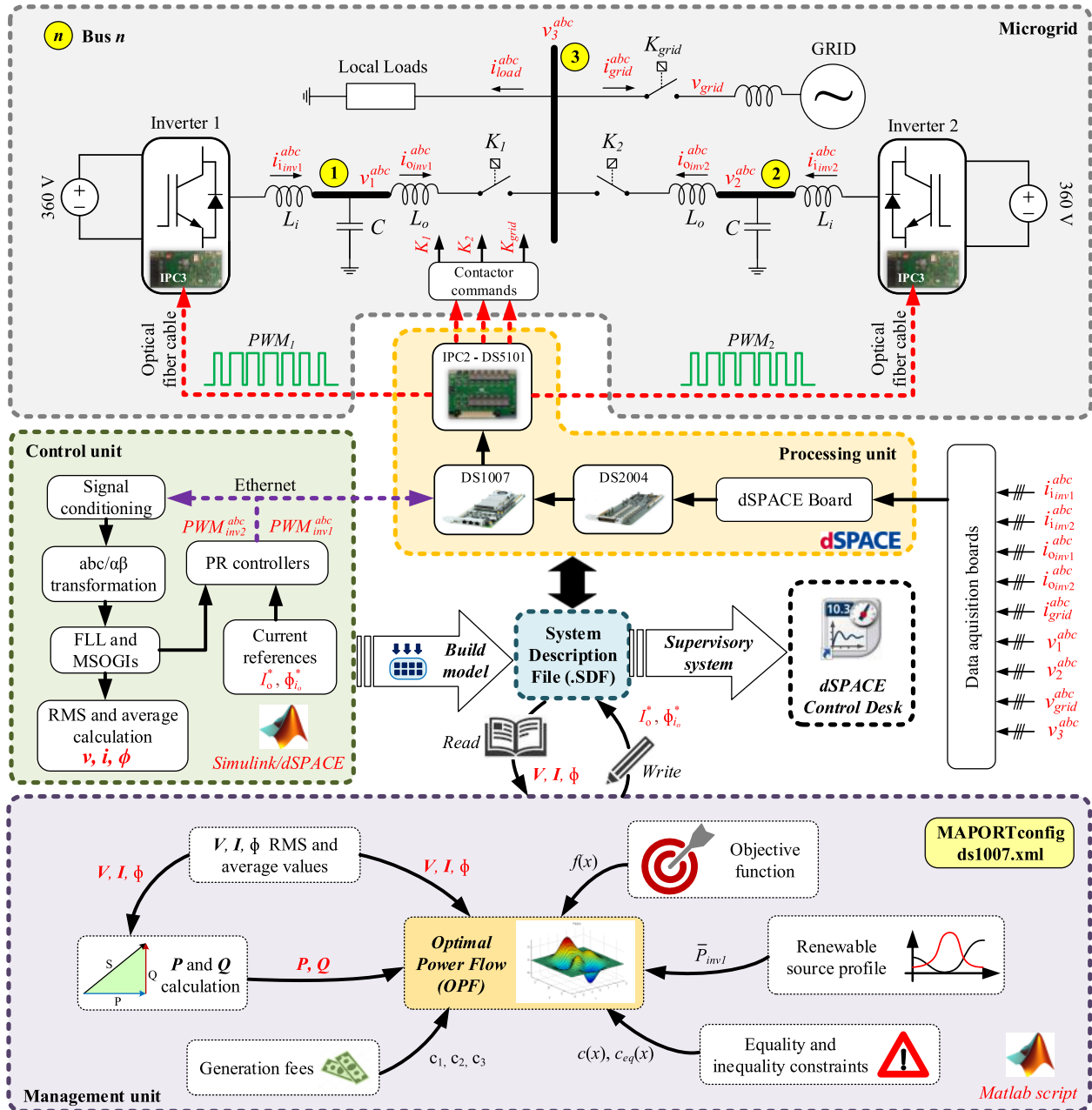
FIGURE 1. Microgrid general diagram with the proposed EMS.

three-phase currents of the LCL filters flowing through the input inductors (L_i) are $i_{i_{inv1}}^{abc}$ and $i_{i_{inv2}}^{abc}$, whereas those flowing through the output inductors (L_o) are $i_{o_{inv1}}^{abc}$ and $i_{o_{inv2}}^{abc}$. In the proposed approach, the three-phase voltages measured on buses 1, 2 and 3 correspond to v_1^{abc}, v_2^{abc} and v_3^{abc}, and the current flowing through the grid is represented by i_{grid}^{abc}. Local loads are connected to the bus 3 and their three-phase currents are denoted as i_{load}^{abc}. Moreover, the voltage v_{grid}^{abc} is used to synchronize and connect the inverters to the grid. The circuit breakers K_1 and K_2 can be closed to form the MG, while the circuit breaker K_{grid} is responsible for switching the MG between grid-tied and stand-alone operation modes.

The design of controllers is performed according to the procedures shown in [29].

III. PROPOSED ENERGY MANAGEMENT SYSTEM

The proposed EMS structure is composed by a data processing unit and a control unit, both running at a frequency of 10.8 kHz, along with a low-frequency energy management unit which runs at 0.1 Hz as illustrated in Fig. 1. The EMS operates by updating the MG energy resources references with a fixed time-step, named as T_{EMS}, in an online scheme. The solution of an optimization problem yields proper values for the references of the EMS.
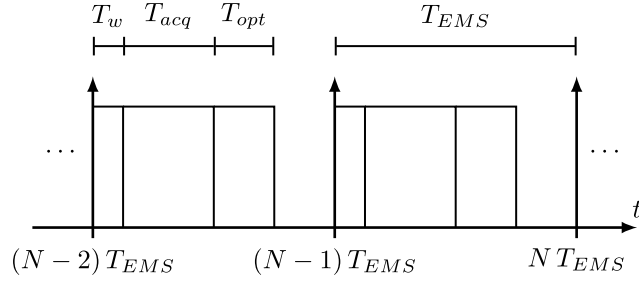
FIGURE 2. EMS real-time processing scheme.

FIGURE 3. Calculating the angular frequency and phase difference between two signals.

Considering that N indicates the current iteration of the EMS after $N T_{EMS}$ seconds, Fig. 2 illustrates how the entire algorithm is processed in real-time. The upward arrows represent the moments where each iteration starts. At the beginning of each iteration, the processor takes T_w seconds to write the previous iteration optimization results in the variables associated with the inverters reference currents. In the sequence, voltage and current measurements are acquired and the related RMS values are computed, which lasts up to T_{acq} seconds. The current iteration optimization step is then performed in the interval T_{opt} seconds, which is based on the measured values. The corresponding results are written at the beginning of the next iteration.

From Fig. 2, it is possible to conclude that the quantity

$$T_{EMS} - (T_w + T_{acq} + T_{opt}) \tag{1}$$

gives the idle time that prevents the EMS algorithm from losing its real-time synchronization. In this case, the constraint

$$T_w + T_{acq} + T_{opt} \leq T_{EMS} \tag{2}$$

must be observed to ensure the EMS proper operation.

A. DATA PROCESSING UNIT

In this unit, the measured data are processed, the control signals are calculated and sent to the inverters, and the commands are sent to the breakers K_1, K_2 and K_{grid}. It contains a processor board DS1007, which is responsible for processing the entire algorithm, a high-speed analog-to-digital board DS2004 for analog signals acquisition, and a digital waveform output board DS5101, which is used to generate the pulse width modulation (PWM) signals to the inverters.

B. CONTROL UNIT

The control unit is embedded in the real-time platform dSPACE 1007, where the signal conditioning, the second order generalized integrator (SOGI)-based fundamental frequency estimation algorithm, the frequency locked loop (FLL) algorithm and the proportional-resonant controllers (PRs) are run along with the RMS and average currents, voltages and phases values computation. For all control steps, the Simulink/MATLAB environment is used to produce the system description file (SDF) according to the MG description.
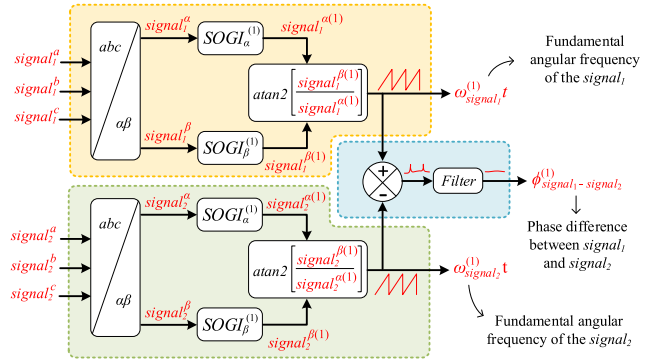
The buses 1, 2 and 3 voltages measurements ($\boldsymbol{v}$), currents measurements ($\boldsymbol{i}$) and phases displacements ($\boldsymbol{\phi}$) are defined as

$$\boldsymbol{v} = [v_1^{(1)} \ v_2^{(1)} \ v_3^{(1)}] \tag{3}$$

$$\boldsymbol{i} = [i_{o_{inv1}}^{(1)} \ i_{o_{inv2}}^{(1)} \ i_{load}^{(1)} \ i_{grid}^{(1)}] \tag{4}$$

$$\boldsymbol{\phi} = [\phi_{v_1}^{(1)} \ \phi_{v_2}^{(1)} \ \phi_{v_3}^{(1)} \ \phi_{i_{o_{inv1}}}^{(1)} \ \phi_{i_{o_{inv2}}}^{(1)} \ \phi_{i_{grid}}^{(1)} \ \phi_{i_{load}}^{(1)}$$
$$\times \phi_{v_1-i_{o_{inv1}}}^{(1)} \ \phi_{v_2-i_{o_{inv2}}}^{(1)} \ \phi_{v_3-i_{grid}}^{(1)} \ \phi_{v_3-i_{load}}^{(1)}] \tag{5}$$

where $\phi_{v_1-i_{o_{inv1}}}^{(1)}$ and $\phi_{v_2-i_{o_{inv2}}}^{(1)}$ are the phases between the inverters 1 and 2 capacitors voltages and inductors L_o currents, respectively. The phase displacements $\phi_{v_3-i_{grid}}^{(1)}$ and $\phi_{v_3-i_{load}}^{(1)}$ are between the PCC voltage and the grid and load currents, respectively. Furthermore, the phase displacements $\phi_{v_1}^{(1)}, \phi_{v_2}^{(1)}, \phi_{v_3}^{(1)}, \phi_{i_{o_{inv1}}}^{(1)}, \phi_{i_{o_{inv2}}}^{(1)}, \phi_{i_{grid}}^{(1)}$ and $\phi_{i_{load}}^{(1)}$ are referenced to the signal $v_{grid}^{(1)}$. The index (1) refers to the fundamental frequency.

From $\boldsymbol{v}$, $\boldsymbol{i}$ and $\boldsymbol{\phi}$, it is possible to calculate the RMS voltages on each bus, the RMS currents and the average phase displacements, which are denoted as

$$\boldsymbol{V} = [V_1 \ V_2 \ V_3] \tag{6}$$

$$\boldsymbol{I} = [I_{o_{inv1}} \ I_{o_{inv1}} \ I_{load} \ I_{grid}] \tag{7}$$

$$\boldsymbol{\Phi} = [\Phi_{v_1} \ \Phi_{v_2} \ \Phi_{v_3} \ \Phi_{i_{o_{inv1}}} \ \Phi_{i_{o_{inv2}}} \ \Phi_{i_{grid}} \ \Phi_{i_{load}}$$
$$\times \Phi_{v_1-i_{o_{inv1}}} \ \Phi_{v_2-i_{o_{inv2}}} \ \Phi_{v_3-i_{grid}} \ \Phi_{v_3-i_{load}}]. \tag{8}$$

As shown in Fig. 3, the extraction of the angular frequency, denoted as $\omega_{signal_1}^{(1)}$, and the phase difference between $signal_1$ and $signal_2$, denoted as $\phi_{signal_1-signal_2}^{(1)}$, are calculated in the stationary reference frame ($\alpha\beta$) by the SOGI algorithm. In order to obtain the grid voltage fundamental frequency ($\omega_{v_{grid}}^{(1)}$), a FLL procedure is used along with the SOGI, forming the SOGI-FLL. Further details about SOGI and FLL structures can be obtained in [30].

The inverters control loops are implemented in the $\alpha\beta$ frame, as presented in Fig. 4. The control structure is based on the PR voltage and current controllers, which can be designed following the procedure in [31]. When the inverters operate in the voltage control mode, the voltage across the LCL filter
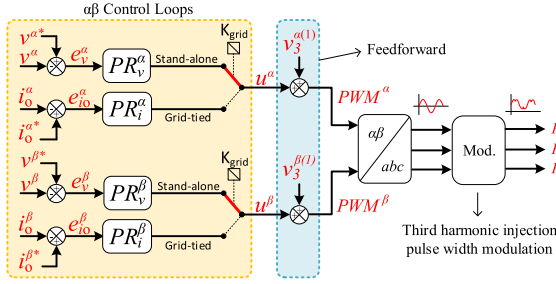
FIGURE 4. Inverter control loops in the $\alpha\beta$ reference frames.

capacitor is adjusted and synchronized with the main grid according to the references

$$v^{\alpha*} = \sqrt{2}V^*cos(\omega_{v_{grid}}^{(1)}t) \tag{9}$$

$$v^{\beta*} = \sqrt{2}V^*sin(\omega_{v_{grid}}^{(1)}t) \tag{10}$$

in which V^* is the root mean square (RMS) phase-to-neutral grid voltage reference value. In addition, the voltage control mode is also used to provides MG voltage and frequency regulations in the stand-alone mode.

In the grid-tied mode, both inverters are set to operate in current control mode, since the voltage and frequency are defined by the main grid. In the current control mode, the current references are calculated by optimization, which correspond to

$$i_o^{\alpha*} = \sqrt{2}I_o^*cos(\omega_{i_o}^{(1)}t + \Phi_{i_o}^*) \tag{11}$$

$$i_o^{\beta*} = \sqrt{2}I_o^*sin(\omega_{i_o}^{(1)}t + \Phi_{i_o}^*) \tag{12}$$

where $\omega_{i_o}^{(1)}$ is the fundamental angular frequency of the current flowing through the inductor L_o, extracted from the SOGI-FLL algorithm, I_o^* and $\Phi_{i_o}^*$ are the OPF solution, obtained in the management unit, which is described next.

C. MANAGEMENT UNIT

The optimization algorithm, responsible for the MG energy management, runs on this unit. It is implemented in a MAT-LAB script and yields the solution of the OPF problem established according to the flowchart in Fig. 5.

From the RMS and the average values, denoted by V, I and Φ, the active and reactive powers of the inverters, the load and the main grid, which are named as

$$P = [P_{inv1}\ P_{inv2}\ P_{load}\ P_{grid}] \tag{13}$$

$$Q = [Q_{inv1}\ Q_{inv2}\ Q_{load}\ Q_{grid}] \tag{14}$$

can be calculated.

From breaker K_{grid} current state, the MG operation mode is checked. In the sequence, the optimization problem initial conditions vector, which is denoted as x_0, is updated by using (6), (7), (8), (13) and (14). For the grid-tied mode, x_0 is given as

$$x_0(grt) = [P_{inv1}\ Q_{inv1}\ P_{grid}\ Q_{grid}\ V_1\ \Phi_{v_1}$$
$$\times V_3\ \Phi_{v_3}\ P_{inv2}\ Q_{inv2}\ V_2\ \Phi_{v_2}\ SoC] \tag{15}$$

and, for the stand-alone mode, it is

$$x_0(sta) = [P_{inv1}\ Q_{inv1}\ V_1\ \Phi_{v_1}\ V_3\ \Phi_{v_3}$$
$$\times P_{inv2}\ Q_{inv2}\ V_2\ \Phi_{v_2}\ SoC]. \tag{16}$$

The vector x_0 corresponds to the system real operating point at the moment that the optimization is performed. After the vector x_0 is updated, the OPF problem is executed according to the power flow equations between buses j and k, which are

$$P_{jk} = G_{jk}V_j^2 - G_{jk}V_jV_kcos(\Phi_{v_j} - \Phi_{v_k})$$
$$+ -B_{jk}V_jV_ksen(\Phi_{v_j} - \Phi_{v_k}) \tag{17}$$

$$Q_{jk} = -B_{jk}V_j^2 + B_{jk}V_jV_kcos(\Phi_{v_j} - \Phi_{v_k})$$
$$+ -G_{jk}V_jV_ksen(\Phi_{v_j} - \Phi_{v_k}) \tag{18}$$

where G_{jk} and B_{jk} are the line conductance and susceptance between j and k buses, respectively. Other inputs of the OPF problem, which are properly discussed in Section V, are the renewable source profile along with the inverters and the grid generation fees, denoted as c_1, c_2 and c_3, respectively.

If the convergence of the OPF reaches the specified tolerance, the algorithm computes the RMS current and phase displacement references for each inverter, yielding the optimization problem solution denoted as x.

It is important to state that the OPF is executed by the `fmincon` MATLAB solver, which finds the minimum of a constrained nonlinear multi-variable function. For solving the optimization problem, the sequential quadratic programming (SQP) algorithm is used. At each iteration, an approximation of the Hessian of the Lagrangian function using a quasi-Newton updating rule is performed. This is then used to generate a quadratic programming sub-problem whose solution is employed to form a search direction for a line search procedure. In this way, the SQP algorithm implemented in this work preserves the optimal characteristic of the computed solutions since it minimizes the Lagrangian by following decreasing directions until the first order optimality measure reaches a given tolerance. More details about the SQP algorithm can be found in [32].

The optimization horizon defined for the energy management is named as H, the control level sampling time as T_s and the renewable source profile sampling rate as T_{real}. The management unit is scaled down from T_{real} to T_{EMS}, allowing the optimization to run H/T_{real} times across the period H, according to **aux** in Fig. 5. The values T_{real} and H are expressed in hours, whereas T_{EMS} and T_s in seconds.

For the purpose of keeping a consistent updating time of T_{EMS} seconds, the algorithm waits until the **cont** counter reaches the defined T_{EMS}/T_s value, which allows the references to be written in the SDF. As a protection mechanism, if the OPF problem converges to an infeasible point, the algorithm maintains the current references previous values.

As for the communication link, the data traffic between the control unit and the management unit is established only by the RMS voltages on each bus, the RMS currents and
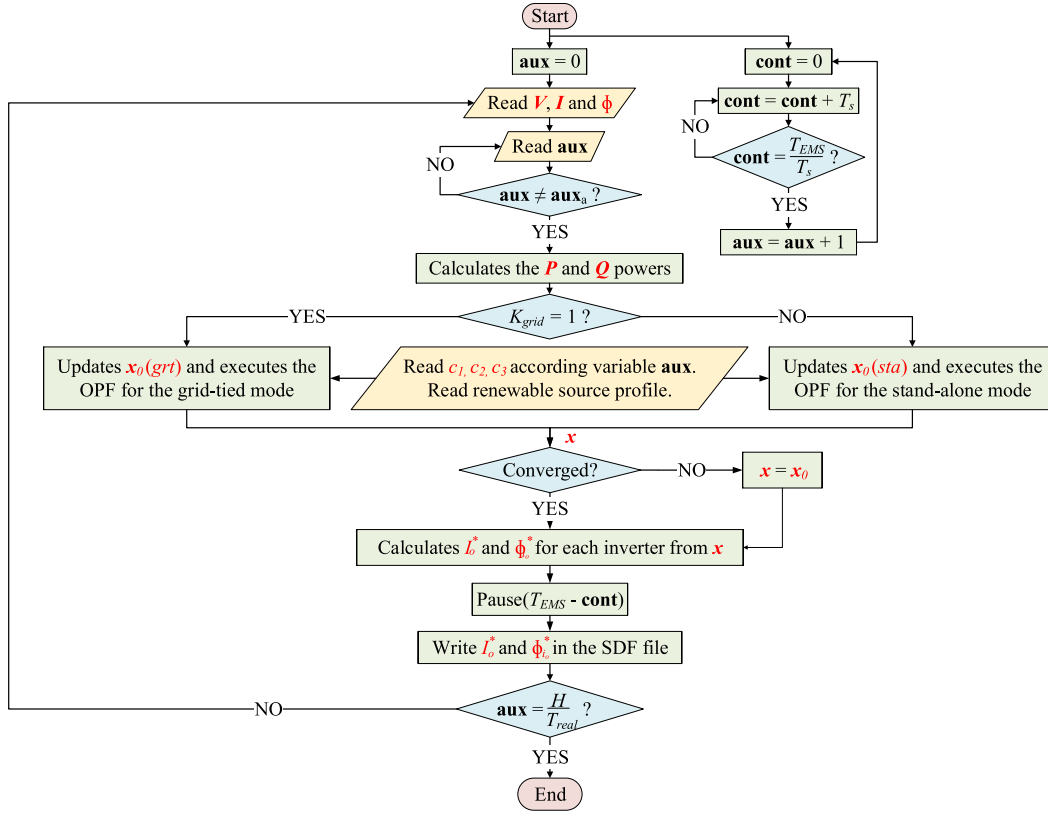
FIGURE 5. MG energy management flowchart.

the average phase displacements, which are denoted as V, I and Φ, respectively. In this work, the amount of data in the communication link for the MG studied is small, hence data congestion and additional delays are not introduced by the proposed EMS implementation strategy. Nevertheless, if vast communication is required, the event trigger or data-driven strategy presented in [11] and [12] are interesting solutions to successfully address communication issues.

IV. OPTIMIZATION PROBLEM FORMULATION

The optimization problem is formulated according to a main objective function, the mth objective function, the equality and inequality constraints, which are denoted as $f_1(x), f_m(x)$, $c_{eq}(x)$ and $c(x)$, respectively. It is important to state that both the equality and inequality constraints are responsible for establishing the system behavior. The optimization method used in this work is the ϵ-constraint method, which allows to treat a problem with multiple objectives in a mono-objective way. The optimization problem is thus formulated as follows [18]:

Minimize $f_1(x)$

such that $f_m(x) \leq \epsilon_m, \quad m = 2, 3, \ldots, n$

$c_{eq}(x) = 0$

$c(x) \leq 0$

where ϵ_m is the mth objective function upper limit and n is the number of objectives.

In the proposed strategy, $n = 2$, which yields objective functions $f_1(x)$ and $f_2(x)$. As j starts from 2, hence only ϵ_2 is used. In this way, $f_1(x)$ is minimized and $f_2(x)$ is defined as an inequality constraint.

A. OBJECTIVE FUNCTION

In this work, the considered objective functions are the MG total generation cost and the active power losses in the LCL filter of each inverter.

1) TOTAL GENERATION COST

The MG total generation cost is represented by the function

$$f_1(x) = c_1 P_{inv1} + c_2 P_{inv2} + c_3 P_{grid} \qquad (19)$$

where the generation fees c_1, c_2, and c_3, expressed in R\$/pu, correspond to the assigned gain for each analyzed scenario. When the MG operates in the stand-alone mode ($K_{grid} = 0$), $c_3 = 0$ and $P_{grid} = 0$.

2) ACTIVE POWER LOSSES

The connection lines among the buses are represented by L_o and their active power losses equations are inserted in the optimization problem objective function. The active power losses can be defined as

$$f_2(x) = \mathcal{P}_{inv1} + \mathcal{P}_{inv2} \qquad (20)$$

in which the individual losses can be calculated via (17), such that

$$\mathcal{P}_{inv1} = P_{13} + P_{31} \tag{21}$$

$$\mathcal{P}_{inv2} = P_{23} + P_{32}. \tag{22}$$

B. OPERATIONAL CONSTRAINTS

The optimization problem constraints correspond to the equations that describe the MG model and also the MG limits, which are defined by equality and inequality constraints, $c_{eq}(\boldsymbol{x})$ and $c(\boldsymbol{x})$, respectively.

1) EQUALITY CONSTRAINTS - $c_{eq}(\boldsymbol{x})$

These are based on the power flow equations of each bus, the MG bus references equations and the battery state of charge SoC, such as

$$P_{inv1} - P_{13} = 0 \tag{23}$$

$$Q_{inv1} + Q_{13} = 0 \tag{24}$$

$$P_{inv2} - P_{23} = 0 \tag{25}$$

$$Q_{inv2} + Q_{23} = 0 \tag{26}$$

$$P_{31} + P_{32} + P_{load} + P_{grid} = 0 \tag{27}$$

$$Q_{31} + Q_{32} + Q_{load} + Q_{grid} = 0 \tag{28}$$

$$V_{ref} - V_{ref_a} = 0 \tag{29}$$

$$\Phi_{V_{ref}} - \Phi_{V_{ref_a}} = 0 \tag{30}$$

$$SoC - SoC_a + \Delta_{SoC} = 0 \tag{31}$$

where

$$\Delta_{SoC} = 100 \frac{P_{inv1} T_{real}}{\overline{P}_{inv1} T_D} \tag{32}$$

V_{ref_a} and $\Phi_{v_{ref_a}}$ are the RMS voltage and the average phase displacement references measured at the moment in which the optimization is performed, respectively. The previous and the current states of charge are SoC_a and SoC, respectively, and T_D is the period of the total battery charge/discharge (100% SoC variation), expressed in hours.

The positive signals in (24) and (26) are related to the reactive power flow convention, where $Q < 0$ indicates that the inverter is generating reactive power, while $Q > 0$ indicates it is consuming. The constraints (29) and (30) are associated with the reference bus to ensure that, after the optimization finishes, the RMS V_{ref} and the average phase displacement Φ_{ref} remain the same. Considering that the reference bus changes according to the MG operation, in the grid-tied mode ($K_{grid} = 1$) the reference is established by the grid resulting in $V_{ref} = V_3$ and $\Phi_{V_{ref}} = \Phi_{v_3}$. On the other hand, in the stand-alone mode ($K_{grid} = 0$), the bus 2 is set to the reference bus, using voltage and frequency control. This bus is related to a dispatchable source, represented by the inverter 2 and defined by $V_{ref} = V_2$ and $\Phi_{V_{ref}} = \Phi_{v_2}$.

2) INEQUALITY CONSTRAINTS - $c(\boldsymbol{x})$

These constraints are related to the MG boundaries, which are the sources generation capacity, as well as the buses

voltages limits, and are given by

$$P_{inv1}^2 + Q_{inv1}^2 \le \overline{S}_{inv1}^2 \tag{33}$$

$$P_{inv2}^2 + Q_{inv2}^2 \le \overline{S}_{inv2}^2 \tag{34}$$

$$P_{grid}^2 + Q_{grid}^2 \le \overline{S}_{grid}^2 \tag{35}$$

$$\underline{P}_{inv1} \le P_{inv1} \le \overline{P}_{inv1} \tag{36}$$

$$\underline{P}_{inv2} \le P_{inv2} \le \overline{P}_{inv2} \tag{37}$$

$$\underline{V}_1 \le V_1 \le \overline{V}_1 \tag{38}$$

$$\underline{\Phi}_{v_1} \le \Phi_{v_1} \le \overline{\Phi}_{v_1} \tag{39}$$

$$\underline{V}_2 \le V_2 \le \overline{V}_2 \tag{40}$$

$$\underline{\Phi}_{v_2} \le \Phi_{v_2} \le \overline{\Phi}_{v_2} \tag{41}$$

$$\underline{SoC} \le SoC \le \overline{SoC} \tag{42}$$

in which, $\overline{S}_{inv1}$, $\overline{S}_{inv2}$ and $\overline{S}_{grid}$ are the maximum apparent power per phase of the inverters and the grid, respectively, $\underline{P}_{inv1}$, $\underline{P}_{inv2}$, $\overline{P}_{inv1}$ and $\overline{P}_{inv2}$ are the inverters lower and upper active power limits, $\underline{V}_1$, $\underline{V}_2$, $\underline{\Phi}_{v_1}$, $\underline{\Phi}_{v_2}$, $\overline{V}_1$, $\overline{V}_2$, $\overline{\Phi}_{v_1}$ and $\overline{\Phi}_{v_2}$ are the lower and upper voltage and phase displacement limits on the buses 1 and 2, and $\underline{SoC}$ and $\overline{SoC}$ are the lower and upper state of charge limits.

C. ADAPTIVE PENALIZATION FACTOR

Some papers address the problem of the influence of the battery power gradient on the battery lifetime and propose strategies to limit its fast power transients [8], [17]. In order to mitigate this problem, in [8], it was proposed the inequality constraint

$$|P_B - P_{B_a}| \le \overline{\Delta}_P \tag{43}$$

with

$$\overline{\Delta}_P = K \overline{P}_B \tag{44}$$

where $\overline{\Delta}_P$ is the battery maximum power gradient, P_{B_a} is the power produced by the battery at the previous step, $\overline{P}_B$ is the battery maximum power and K is the penalization factor, which was chosen as 0.15. However, if K is fixed, whenever $P_B \ge K\overline{P}_B$ and the SoC is either $\underline{SoC}$ or $\overline{SoC}$, the optimization algorithm fails.

When the SoC reaches the limit $\underline{SoC}$, as exemplified in Fig. 6, the power variation must be equal to $4\overline{\Delta}_P$ such that the storage device output power be null ($P_B = 0$) and the SoC remains at the lower limit imposed by the minimum constraint $\underline{SoC}$. If that is not the case, the SoC will continue to decrease until the point this constraint is violated.

This occurs because when the battery is supplying the maximum power ($P_B = \overline{P}_B$) and its state of charge is minimal ($SoC = \underline{SoC}$), if constraint (43) is achieved, the SoC will be reduced to a value that is lower than $\underline{SoC}$, while P_B remains positive. The same process occurs when the battery is charging with maximum power ($P_B = \underline{P}_B$).

To alleviate this problem, in this work, the use of an adaptive penalization factor K for each storage device operating

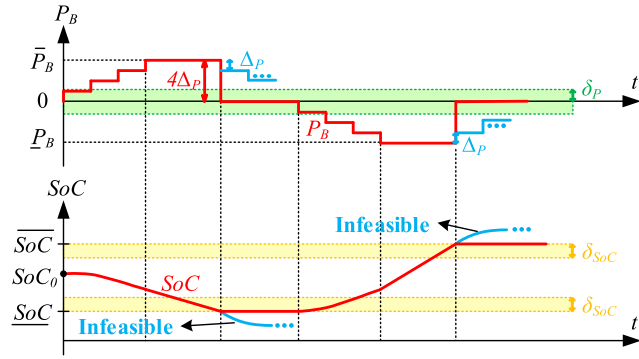**FIGURE 9.** Generation fees with dispatchable sources and storage devices.

FIGURE 6. Behavior of battery active power and SoC (red) with and (blue) without the proposed battery power gradient constraint.
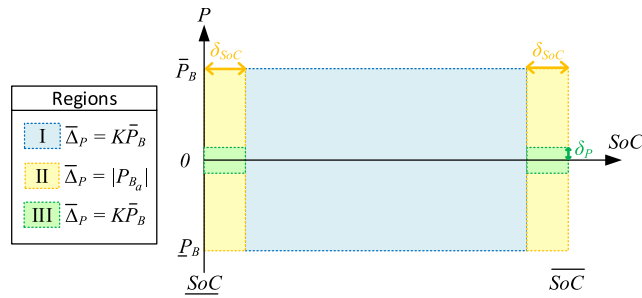

FIGURE 7. Areas of the battery power gradient constraint according to K.
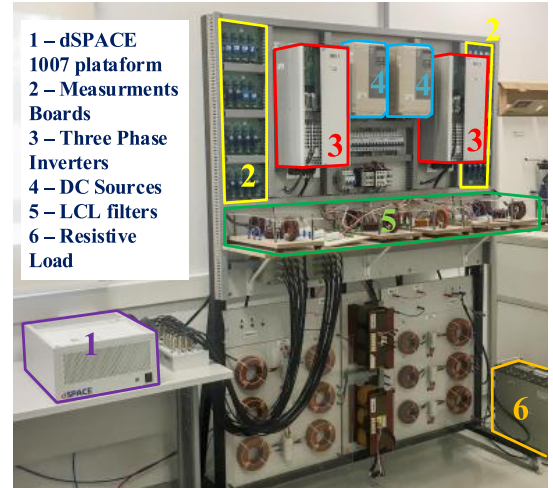
FIGURE 10. Experimental bench.

TABLE 1. Parameters used in the optimization problem.

Parameter	Value	Parameter	Value
$\underline{V}_1, \underline{V}_2, \underline{V}_3$	0.95pu	$\underline{P}_{inv2}$	0W
$\overline{V}_1, \overline{V}_2, \overline{V}_3$	1.05pu	ϵ	0.01
$\underline{\Phi}_{v_1}, \underline{\Phi}_{v_2}, \underline{\Phi}_{v_3}$	$-\pi$rad	T_{real}	$\frac{1}{12}$h
$\overline{\Phi}_{v_1}, \overline{\Phi}_{v_2}, \overline{\Phi}_{v_3}$	πrad	T_D	2h
$\underline{P}_{inv1}, \overline{P}_{inv1}, \overline{S}_{inv1}$	*	T_{EMS}	10s
$\overline{P}_{inv2}, \overline{P}_{load}$	$\frac{1,000}{3}$W	T_s	$\frac{1}{10,800}$s
$\overline{S}_{grid}$	$\frac{2,000}{3}$VA	H	24h
$\overline{S}_{inv2}$	$\frac{1,000}{3}$VA	C	10uF
R_i, R_o	0.12Ω	SoC_0	50%
L_i, L_o	2mH	$\underline{SoC}$	30%
G_{13}, G_{23}	0.2059Ω^{-1}	$\overline{SoC}$	90%
B_{13}, B_{23}	-1.2935Ω^{-1}	$\overline{P}_{load}$	$\frac{1,000}{3}$W

* The limits depends on the scenario analyzed. For the scenario described in the section-V-A, they are $\underline{P}_{inv1} = 0$W, $\overline{P}_{inv1} = \frac{1,000}{3}$W and $\overline{S}_{inv1} = \frac{1,000}{3}$VA, whereas for the scenario described in the section-V-B, they are $\underline{P}_{inv1} = -150$W, $\overline{P}_{inv1} = 150$W and $\overline{S}_{inv1} = 150$VA.
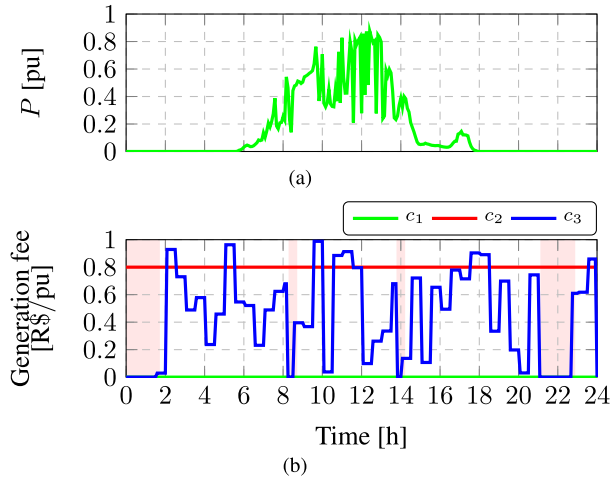

FIGURE 8. Photovoltaic power profile (a) and generation fees (b) for dispatchable and non-dispatchable sources.

point, according to the regions defined in Fig. 7, is proposed. In this case, region-I is delimited by

$$(\underline{SoC} + \delta_{SoC}) \leq SoC \leq (\overline{SoC} - \delta_{SoC}) \qquad (45)$$

where δ_{SoC} corresponds to $|\Delta_{SoC}|$ with the storage device either producing or absorbing maximum active power ($P_B = \overline{P}_B$), which is calculated by

$$\delta_{SoC} = 100\frac{T_{real}}{T_D}. \qquad (46)$$

In region-I, K is constant and the battery maximum power gradient is such that $\overline{\Delta}_P = K\overline{P}_B$. However, when the storage
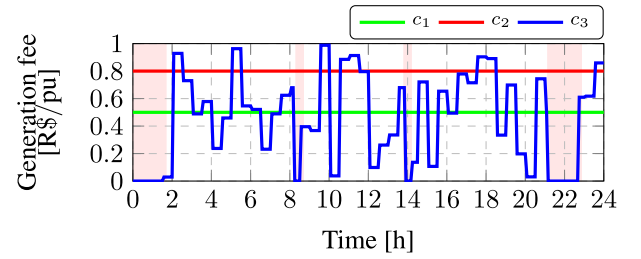
device operating point reaches region-II, $\overline{\Delta}_P$ corresponds to the previous step of the absolute battery power $|P_{B_a}|$. When the SoC is close to either $\underline{SoC}$ or $\overline{SoC}$, the maximum power gradient is relaxed, that is $\overline{\Delta}_P = |P_{B_a}|$, to avoid that the optimization problem solution converges to an infeasible point, as shown in Fig. 6.

Region-III is achieved when the SoC is either $\underline{SoC}$ or $\overline{SoC}$, and P_B has to be zero to avoid violation of constraint (42). The storage device operating point remains in this region
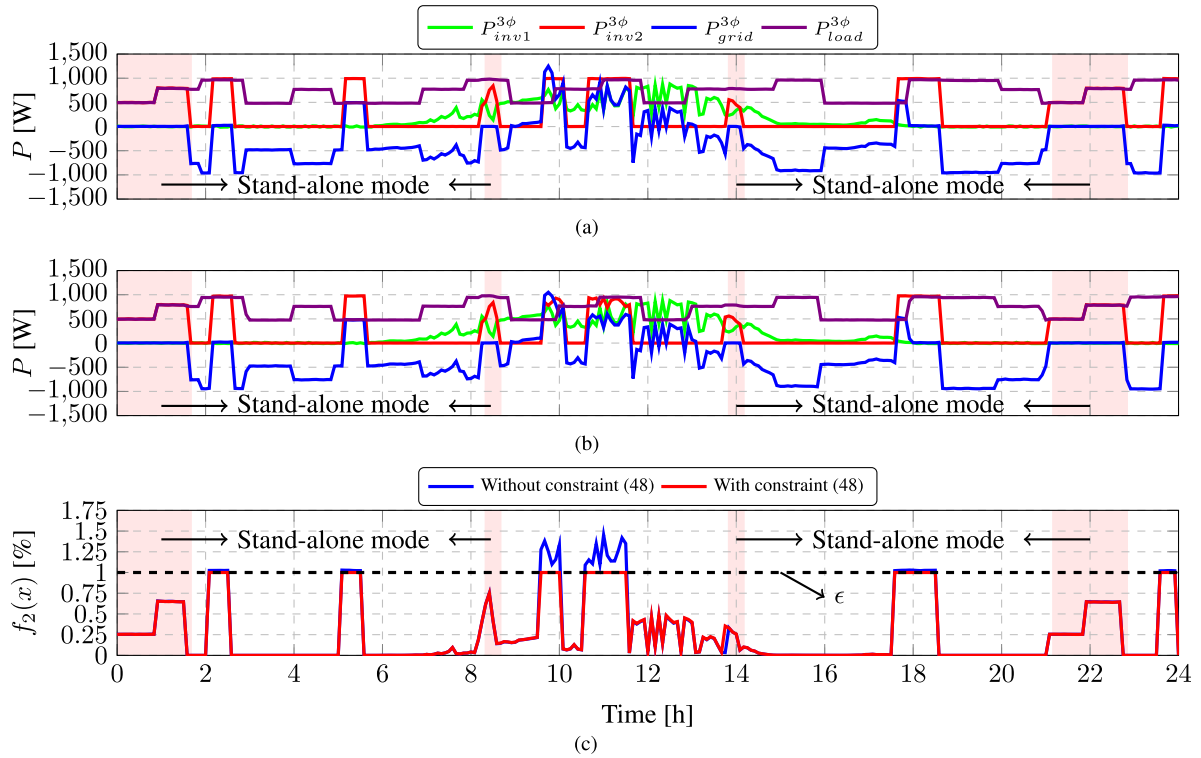
FIGURE 11. Three-phase active power behavior of the inverters, grid and load (a) without and (b) with the constraint (48), and (c) comparison of the MG total losses with and without constraint (48).
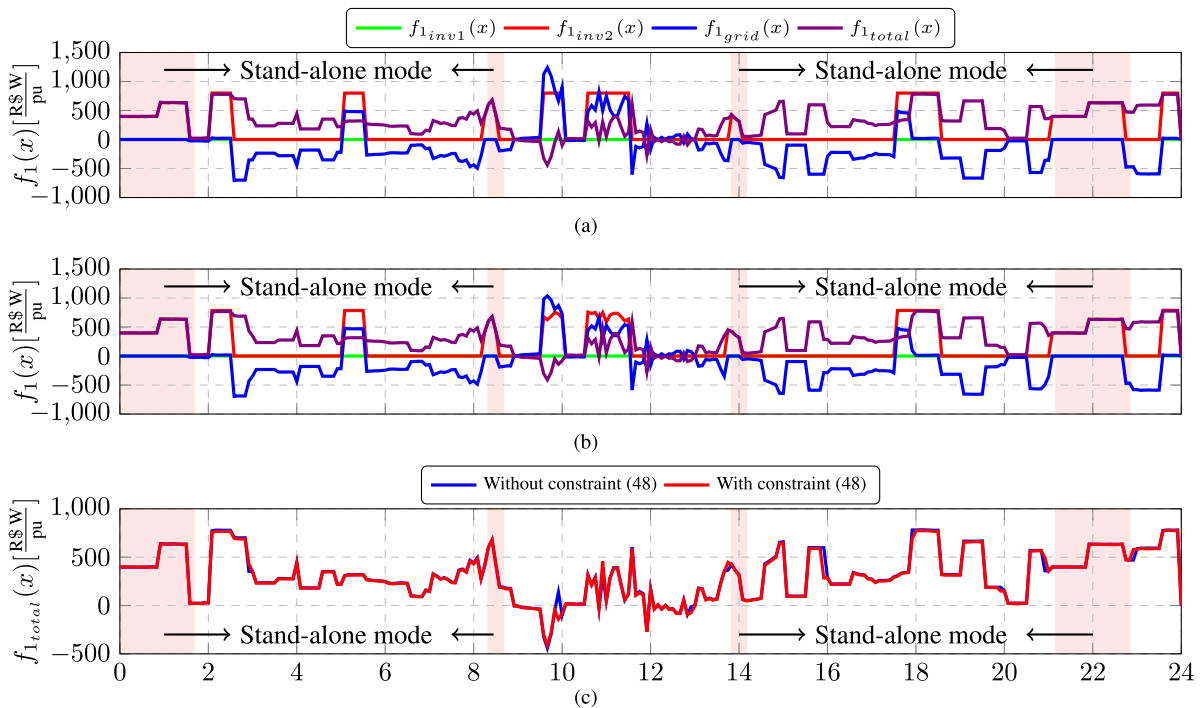

FIGURE 12. Behavior of the MG individual and total cost (a) without and (b) with constraint (48) and (c) a comparison between the total cost for both cases.

until the *SoC* returns to the region-I. Furthermore, region-III limits the power gradient for the next battery charging or discharging process, eliminating fast transients on P_B when $P_{B_a} = 0$.

In order to limit the battery power gradient according to the regions shown in Fig. 7, the constraint

$$[P_B - P_{B_a}]^2 \leq \overline{\Delta}_P{}^2 \tag{47}$$

which is a quadratic form of (43), is inserted into the optimization problem to improve the algorithm convergence.

Additionally, the energy management algorithm uses a constraint on the active power losses which is given as

$$f_2(x) \leq \epsilon \overline{P}_{load} \tag{48}$$

where ϵ is chosen as a percentage of the maximum load of the MG.

V. EVALUATION SCENARIOS

In order to validate the proposed EMS, two scenarios under different operating conditions are evaluated. The analyzed MG parameters are the losses limits, the variable generation costs and the different energy sources topologies when a group of photovoltaic arrays, battery and conventional sources are used.

It is important to state that both grid-tied and stand-alone modes are considered during the scenarios evaluation. In the grid-tied mode, as both inverters operate in current control mode, the voltage and frequency are held by the grid. Upon occurring the transition from grid-tied to stand-alone mode, the inverter 1 is kept in current control mode, while inverter 2 is set to voltage control mode to provide MG voltage and frequency support.

A. DISPATCHABLE AND NON-DISPATCHABLE SOURCES

In this scenario, inverter 1 is a non-dispatchable source and is supplied by a photovoltaic array with a solar profile updated at a 5-min sampling rate, as shown in Fig. 8(a). On the other hand, inverter 2 is a dispatchable energy source capable of supplying power in a controlled way, such as diesel or thermal generators. In this context, Fig. 8(b) presents the generation cost related to the inverters and the grid. The inverter 1 generation cost is considered null ($c_1 = 0$) since it represents a renewable energy source, while the generation cost of inverter 2 is $c_2 = 0.8$. When compared to c_2, the grid generation cost c_3 has a random profile, since it represents the cost variations inside the optimization horizon H.

The highlighted regions in Fig. 8(b), which are defined by $0 \leq t \leq$ 1h40, 8h20 $\leq t \leq$ 8h40, 13h50 $\leq t \leq$ 14h10 and 21h10 $\leq t \leq$ 22h50, correspond to the time intervals at which the MG operates in the stand-alone mode. In these time intervals, the inverter 2 operates in voltage control mode, which maintains the MG voltage and frequency levels.

B. DISPATCHABLE SOURCE AND ENERGY STORAGE DEVICE

In this scenario, inverter 1 is an energy storage device (battery) able to deliver maximum power during two consecutive hours. Additionally, this device has an arbitrary generation fee ($c_1 = 0.5$) in the entire 24h, and it is inserted to penalize
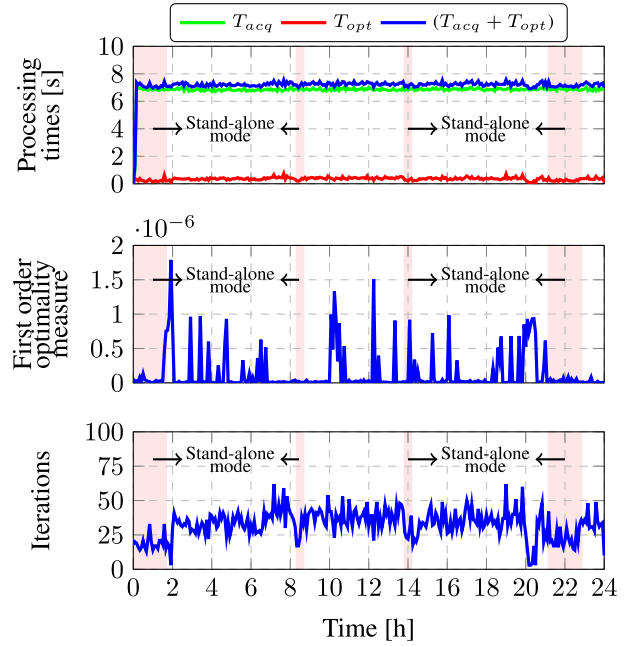

FIGURE 13. Optimization parameters results obtained when running the proposed EMS without considering constraint (48).

the battery discharging process. This fee is needed to preserve the battery lifetime, prioritize its charging process and keep the *SoC* at levels higher than *SoC*.

As in the previous scenario, the regions highlighted in Fig. 9 show the moments where the MG is operating in the stand-alone mode (the same time intervals are considered). Furthermore, inverter 2 corresponds to a dispatchable source with a constant generation fee ($c_2 = 0.8$), while the grid has a variable generation fee, as can be seen in Fig. 9.

VI. EXPERIMENTAL RESULTS

The experimental bench uses two three-phase Danfoss FC 302 inverters, a dSPACE 1007 platform with a 2GHz dual-core processor and a 1GB DRAM memory, and a DS2004 High-Speed A/D measurement board. The complete experimental bench is shown in Fig. 10. The management level is executed by a central computer and implemented in a MATLAB script, which reads the contents in the SDF, executes the optimization algorithm and writes the inverters current references in the same SDF. The controllers run in real-time, while in the management unit the time is scaled down from minutes to seconds (5min:10s). Table 1 presents the system parameters used to solve the optimization problem.

A. DISPATCHABLE AND NON-DISPATCHABLE SOURCES

Considering that inverters 1 and 2 are a photovoltaic array and a dispatchable source, respectively, Fig. 11 shows the behavior of the three-phase active power of these inverters along with the grid and the load profiles, with and without the losses constraint established in (48). The highlighted areas in Fig. 11 correspond to the time intervals at which the MG
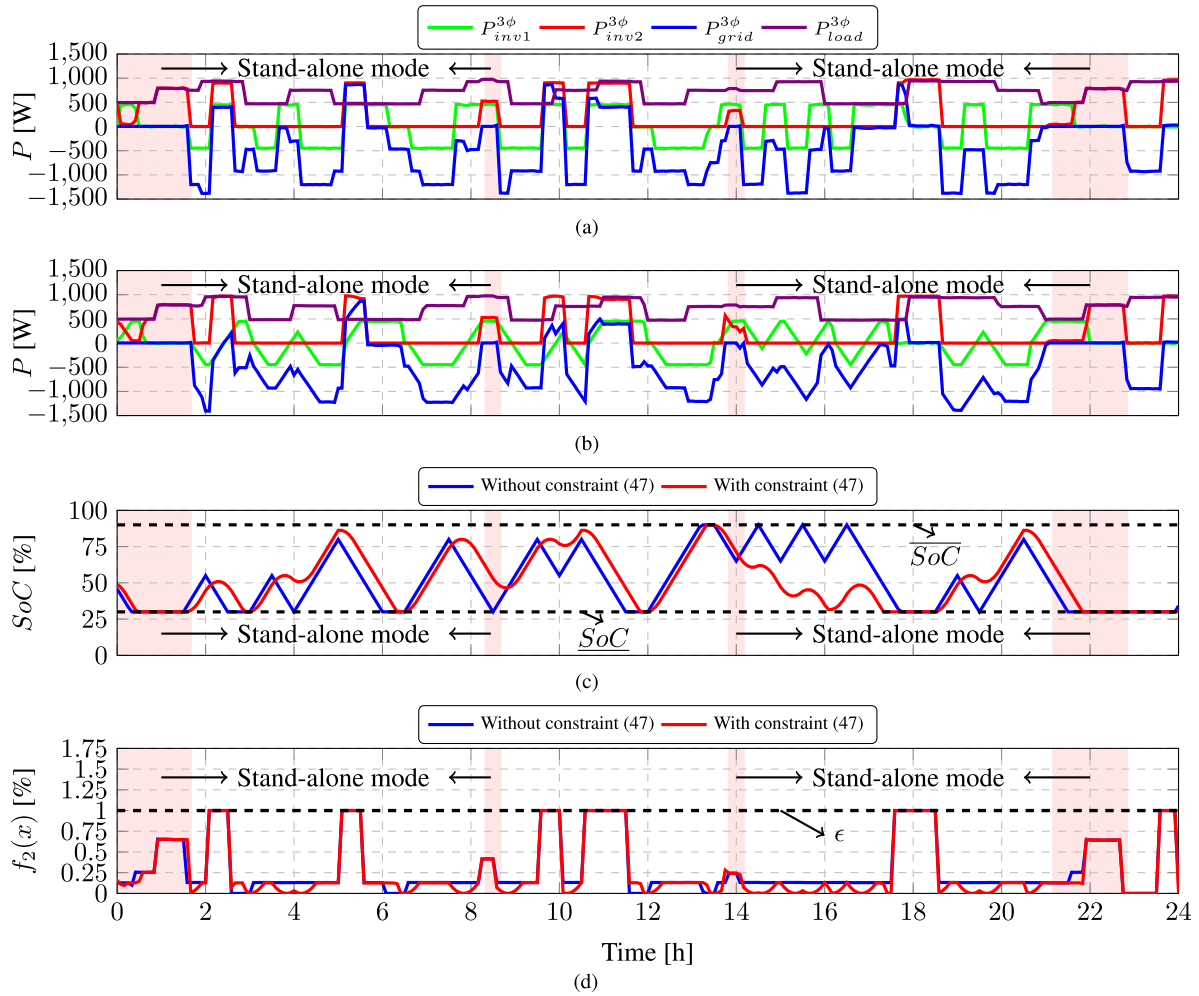
FIGURE 14. Three-phase active power behavior of the inverters, grid and load (a) without and (b) with the power gradient constraint, and the comparison with and without the power gradient constraint (c) states of charge and (d) MG total losses.

operates in the stand-alone mode, that is the active power supplied or absorbed by the grid is zero. During these time intervals, the grid is not available and thus the MG voltage and frequency are established by bus 2, which is set as the reference bus.

Taking into account that the generation fee $c_1 = 0$ for the photovoltaic array, this source is prioritized in terms of power delivery. In this way, the photovoltaic source will operate at the maximum power point whenever the power demanded by the local load is greater than or equal to its maximum generating capacity.

The dispatchable source and grid operate according to the load profile and the fees c_2 and c_3 shown in Fig. 8(b). In Figs. 11(a) and 11(b), when $P_{grid} < 0$ the grid supplies power to the MG, whereas in the moments when $P_{grid} > 0$ the MG is delivering power to the main grid.

The comparison between the MG total electrical losses for both cases is presented in Fig. 11(c). As can be observed, the most significant difference between these cases occurs in the time intervals $9h30 \le t \le 10h$ and $10h30 \le t \le 11h30$.

During these intervals $c_2 < c_3$ in which case the EMS adjusts the inverter 2 to operate in its maximum generation capability without considering constraint (48) in the OPF problem, as can be seen in Fig. 11(a). In this case, the MG is capable of supplying all the active power required by the load and the exceeding energy is delivered to the main grid. Nevertheless, when the constraint (48) is included in the optimization algorithm, as shown in Fig. 11(b), the inverter 2 does not operate in its maximum generation capability. This occurs because, although maximum generation capability is economically desired, the EMS needs to decrease the generated power P_{inv2} to keep the MG total electrical losses below the pre-established ϵ boundary.

The individual generation cost related to both the inverters 1 and 2 sources ($f_{1_{inv1}}$ and $f_{1_{inv2}}$) and the main grid ($f_{1_{grid}}$), along with the total MG generation cost ($f_{1_{total}}$), are presented in Fig. 12. Considering that the inverter 1 is connected to a renewable source, where the generation fee $c_1 = 0$, no generation cost is applied. The cost $f_{1_{total}}$ indicates if the MG is operating either buying or selling energy to the main grid.
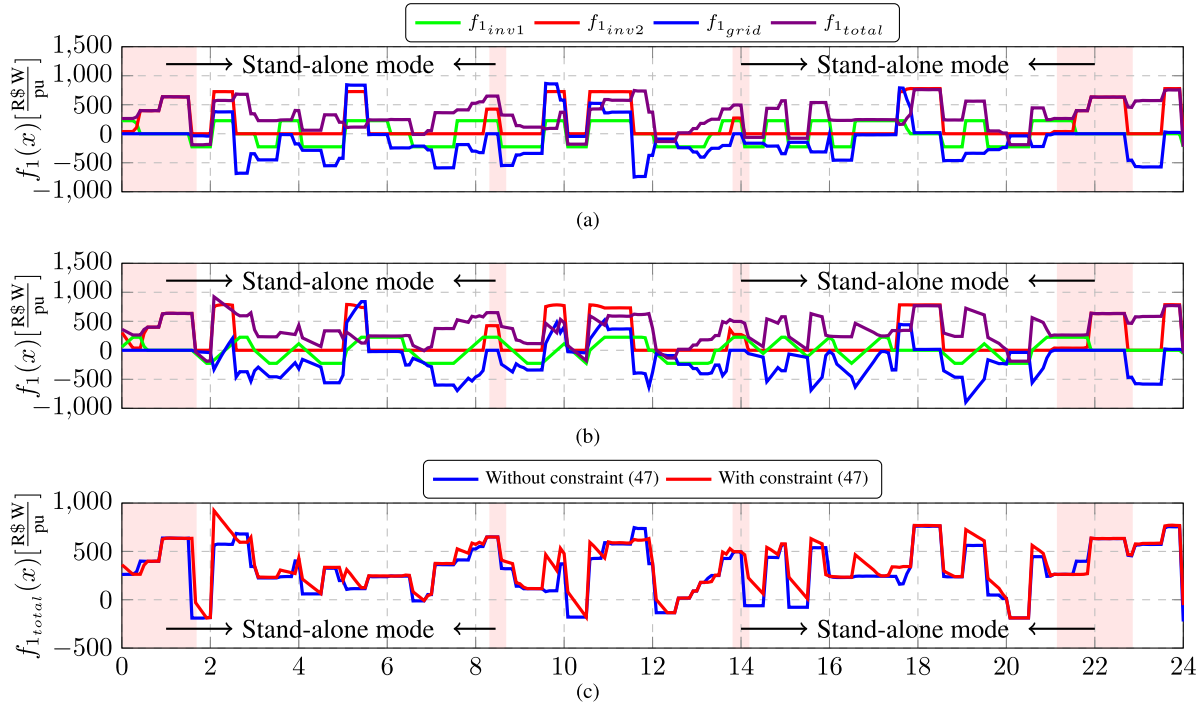
FIGURE 15. Behavior of the MG individual and total cost (a) without and (b) with the constraint (47) and (c) a comparison between the total cost for both cases.

When $f_{1_{total}} < 0$, the total power generated by the sources in this case is greater than that consumed by the local load. Thus, the MG operates in profit, since the exceeding energy is sold to the main grid. On the other hand, when $f_{1_{total}} > 0$, the MG is not self-sufficient, in which case it needs to buy energy from the main grid to keep the local loads fully supplied.

The comparison between the total MG generation cost of both cases, with and without considering constraint (48), is shown in Fig. 12(c). Since the LCL filters inductors resistive losses are relatively small ($R_o = 0.12\Omega$), the active power profiles and the MG total electrical losses are similar, as can be seen in Fig. 11. For this reason, the total cost curves $f_{1_{total}}$ obtained for both cases also describe a similar behavior. However, when the MG losses constraint is inserted, the total generation cost tends to be greater owing to the fact that the EMS starts now operating not only focusing on the best economic approach, but also on attaining the boundaries introduced by constraint (48).

In Fig. 13, it is possible to observe the experimental measurements of the processing times related to the EMS real-time operation, the first order optimality measure and the optimization algorithm iterations when the case in Fig. 11(a) is tested. When testing the other case, which is presented in Fig. 11(b), the results are similar. As discussed in the Fig. 2 description, the EMS execution time is calculated as $T_w + T_{acq} + T_{opt} \approx T_{acq}$, which is kept around 7s along the entire 24 hours. The value of T_w is fixed at 50ms and $T_{opt} < 1s$. Since $T_{EMS} = 10s$, the EMS is consistently run within a 10s time-frame, which ensures a fixed updating rate

of the reference variables. For all operating points, the first order optimality measure is below 2.10^{-6} and the algorithm takes less than 60 iterations to reach convergence.

B. DISPATCHABLE SOURCE AND ENERGY STORAGE DEVICE

Considering that the inverter 1 is supplied by an energy storage device and the inverter 2 is a dispatchable source, Fig. 14 shows the behavior of the three-phase active power of these inverters along with the grid and the load profiles, with and without the power gradient constraint established in (47), in which, in this scenario, P_B and P_{B_a} correspond to P_{inv1} and P_{inv1_a}, respectively. In both cases, the storage device initial state of charge is $SoC_0 = 50\%$. In this case, for example, the first highlighted region, which starts at $t = 0h$, shows that the battery is delivering energy to the local load, since $c_1 < c_2$. When the state of charge reaches its lower limit, that is $\underline{SoC} = 30\%$, the battery stops delivering power and the load starts to be fully supplied by the dispatchable source.

In Fig. 14(a), it is possible to see the abrupt variations occurring in the power P_{inv1}, which alternates instantly between the storage device charge and discharge processes. This is observed due to the fact that when the gradient constraint (47) is not considered, the power transients either produced or consumed by the battery becomes free to alternate between the upper and the lower allowed limits, which are $\overline{P}_{inv1}$ and $\underline{P}_{inv1}$.

In order to suppress fast transients that might compromise the storage device lifetime, constraint (47) is inserted in
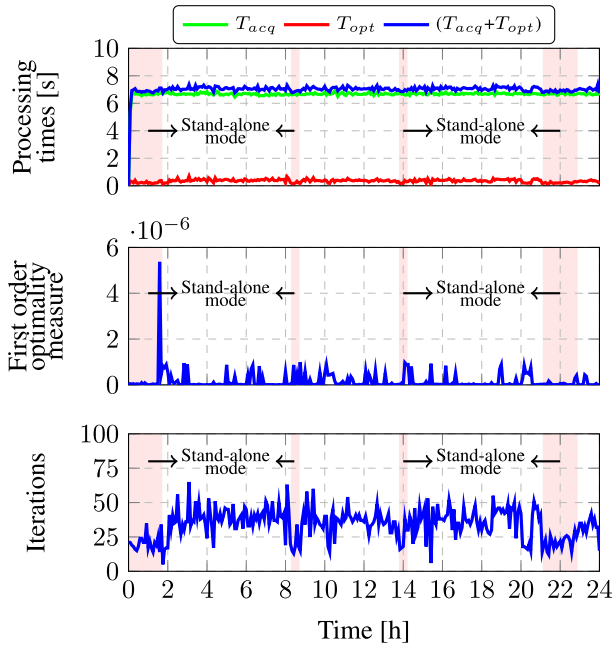
FIGURE 16. Optimization parameters results obtained when running the proposed EMS without considering the constraint (47).

the optimization problem. The penalization factor considered was $K = 0.25$, which limit the storage device power gradient in 25% of its maximum power between two consecutive optimization algorithm executions. The behaviors of the three-phase active powers, the battery state of charge and the total MG electrical losses are presented in Fig. 14.

The comparison between the battery state of charge for both cases, without and with constraint (47), is shown in Fig.14(c). Note that after including the constraint, the transition between the charge and the discharge processes of the battery were smooth due to the power gradient limitation.

In both cases, the losses constraint represented by (48) is maintained in the OPF solution, as can be seen in Fig.14(d). Note that the losses remain below the pre-established ϵ value ($\epsilon = 1$%) along all the universe of discourse. In addition, with the power gradient constraint, smaller total losses in the MG and decreased battery degradation in its lifetime are guaranteed.

The sources and the main grid individual generation cost, along with the MG total generation cost, are shown in Fig. 15. From the comparison presented in Fig. 15(c), where the total MG generation cost with and without constraint (47) is considered, it is possible to see that greater values of cost $f_{1_{total}}$ are attained when the constraint is inserted. Knowing that this constraint limits the power generated by the battery, the cost increases since part of the power demanded by the local load starts to be provided by either inverter 2 or the main grid, which have a higher generation fee than the battery.

In Fig. 16, it is presented the parameters related to the EMS execution time, the first order optimality measure and the optimization algorithm iterations when constraint (47) is not applied. As observed in the previous

scenario (see Section VI-A), the EMS execution time was around 7s. As can be seen, along the entire 24 hours the first order optimality measure was kept below $6 \cdot 10^{-6}$ and the algorithm takes less than 60 iterations to reach convergence. Since the optimization parameters results presented in Fig. 16, which are related to the case in Fig. 14(a), describe a similar behavior compared to those obtained when the case in Fig. 14(b) was tested, only the former results are presented.

VII. CONCLUSION

In this work, an energy management system based on an OPF problem for MG, which allows operation in both grid-tied and stand-alone modes, was presented. The optimization problem was solved by the ϵ-constraint method and prioritized the generation cost minimization while ensuring that the active power losses remained below a pre-established value ϵ and also suppressing damaging fast transients in the energy storage device.

In order to validate the proposed EMS, two scenarios were analyzed under different types of sources, such as dispatchable and non-dispatchable sources, and storage devices. For the two evaluated scenarios, the first order optimality measure was kept below 6×10^{-6} during the entire observed 24 hours, which demonstrate the effectiveness of the proposed approach.

According to the experimental results, the proposed EMS was capable of smoothing fast transitions during batteries charge and discharge processes. Considering that batteries are expensive components in MGs, the implemented strategy, which also focuses on the power gradient limitation of storage devices, showed to be an efficient method to approach the MGs energy management, since it allows increasing the battery lifetime.

Although in this work the active power losses in the connection lines are considered to be relatively small (around 1%) due to the sources generation capacities and the LCL filters resistance values, more significant active power losses quantities can be found with other MGs configurations. In this way, it is interesting that an EMS be flexible to permit setting the allowed maximum total losses values.

The proposed EMS kept the current references updating consistently at a 10s fixed rate, as presented in the experimental results. Since the tertiary control layer used in MGs usually have a slow dynamic response, typically reaching the minutes range, the EMS structure presented in this work is also suitable for more complex and larger MGs, which requires a higher algorithm convergence time and, consequently, a higher EMS sampling time.

Overall, the results showed that the proposed approach, which is based on the ϵ-constraint method, yields an effective solution by considering both the MG total electrical losses and the storage device power gradient as constraints in the power flow optimization problem formulation. Although a cost criterion to verify how the battery lifetime is in fact affected by the proposed solution was not defined in this work, it can be treated as a study-case to enrich future

versions of our research. In this case, the benefits introduced by our approach in preserving batteries in a MG can be evaluated.

REFERENCES

[1] M. F. Zia, E. Elbouchikhi, and M. Benbouzid, "Microgrids energy management systems: A critical review on methods, solutions, and prospects," *Appl. Energy*, vol. 222, pp. 1033–1055, Jul. 2018.

[2] A. Bidram and A. Davoudi, "Hierarchical structure of microgrids control system," *IEEE Trans. Smart Grid*, vol. 3, no. 4, pp. 1963–1976, Dec. 2012.

[3] E. Planas, J. Andreu, and J. I. Gárate, I. M. de Alegría, and E. Ibarra, "AC and DC technology in microgrids: A review," *Renew. Sustain. Energy Rev.*, vol. 43, pp. 726–749, Mar. 2015.

[4] K. Balasubramaniam, P. Saraf, R. Hadidi, and E. B. Makram, "Energy management system for enhanced resiliency of microgrids during islanded operation," *Electr. Power Syst. Res.*, vol. 137, pp. 133–141, Aug. 2016.

[5] M. Elsied, A. Oukaour, T. Youssef, H. Gualous, and O. Mohammed, "An advanced real time energy management system for microgrids," *Energy*, vol. 114, pp. 742–752, Nov. 2016.

[6] M. A. Abido and M. Waqar Ahmed, "Multi-objective optimal power flow considering the system transient stability," *IET Gener., Transmiss. Distrib.*, vol. 10, no. 16, pp. 4213–4221, 2016.

[7] C. Deckmyn, T. L. Vandoorn, J. Van de Vyver, J. Desmet, and L. Vandevelde, "A microgrid multilayer control concept for optimal power scheduling and voltage control," *IEEE Trans. Smart Grid*, vol. 9, no. 5, pp. 4458–4467, Sep. 2018.

[8] M. Ruiz-Cortés, E. González-Romera, R. Amaral-Lopes, E. Romero-Cadaval, J. Martins, M. I. Milanés-Montero, and F. Barrero-González, "Optimal charge/discharge scheduling of batteries in microgrids of prosumers," *IEEE Trans. Energy Convers.*, vol. 34, no. 1, pp. 468–477, Mar. 2019.

[9] G. Agundis-Tinajero, N. L. D. Aldana, A. C. Luna, J. Segundo-Ramírez, N. Visairo-Cruz, J. M. Guerrero, and J. C. Vazquez, "Extended-optimal-power-flow-based hierarchical control for islanded AC microgrids," *IEEE Trans. Power Electron.*, vol. 34, no. 1, pp. 840–848, Jan. 2019.

[10] J. B. Almada, R. P. S. Le ao, R. F. Sampaio, and G. C. Barroso, "A centralized and heuristic approach for energy management of an AC microgrid," *Renew. Sustain. Energy Rev.*, vol. 60, pp. 1396–1404, Jul. 2016.

[11] X. Liu, L. Li, Z. Li, X. Chen, T. Fernando, H. H.-C. Iu, and G. He, "Event-trigger particle filter for smart grids with limited communication bandwidth infrastructure," *IEEE Trans. Smart Grid*, vol. 9, no. 6, pp. 6918–6928, Nov. 2018.

[12] S. Li, L. Li, Z. Li, X. Chen, T. Fernando, H. H.-C. Iu, G. He, Q. Wang, and X. Liu, "Event-trigger heterogeneous nonlinear filter for wide-area measurement systems in power grid," *IEEE Trans. Smart Grid*, vol. 10, no. 3, pp. 2752–2764, May 2019.

[13] P. T. Baboli, M. Shahparasti, M. P. Moghaddam, M. R. Haghifam, and M. Mohamadian, "Energy management and operation modelling of hybrid AC–DC microgrid," *IET Gener., Transmiss. Distrib.*, vol. 8, no. 10, pp. 1700–1711, Oct. 2014.

[14] A. C. Luna, N. L. Diaz, M. Graells, J. C. Vasquez, and J. M. Guerrero, "Online energy management system for distributed generators in a grid-connected microgrid," in *Proc. IEEE Energy Convers. Congr. Exposit. (ECCE)*, Sep. 2015, pp. 4616–4623.

[15] M. Marzband, S. S. Ghazimirsaeid, H. Uppal, and T. Fernando, "A real-time evaluation of energy management systems for smart hybrid home microgrids," *Electr. Power Syst. Res.*, vol. 143, pp. 624–633, Feb. 2017.

[16] A. C. Luna, L. Meng, N. L. Diaz, M. Graells, J. C. Vasquez, and J. M. Guerrero, "Online energy management systems for microgrids: Experimental validation and assessment framework," *IEEE Trans. Power Electron.*, vol. 33, no. 3, pp. 2201–2215, Mar. 2018.

[17] W. Shi, X. Xie, C. C. Chu, and R. Gadh, "Distributed optimal energy management in microgrids," *IEEE Trans. Smart Grid*, vol. 6, no. 3, pp. 1137–1146, May 2015.

[18] K. Deb, *Multi-Objective Optimization Using Evolutionary Algorithms*. Hoboken, NJ, USA: Wiley, 2001.

[19] A. H. Fathima and K. Palanisamy, "Optimization in microgrids with hybrid energy systems—A review," *Renew. Sustain. Energy Rev.*, vol. 45, pp. 431–446, May 2015.

[20] B. Zhao, X. Wang, D. Lin, M. Calvin, J. Morgan, R. Qin, and C. Wang, "Energy management of multiple microgrids based on a system of systems

[21] L. Mellouk, A. Aaroud, D. Benhaddou, K. Zine-Dine, and M. Boulmalf, "Overview of mathematical methods for energy management optimization in smart grids," in *Proc. 3rd Int. Renew. Sustain. Energy Conf. (IRSEC)*, 2015, pp. 1–5.

[22] P. Malysz, S. Sirouspour, and A. Emadi, "An optimal energy storage control strategy for grid-connected microgrids," *IEEE Trans. Smart Grid*, vol. 5, no. 4, pp. 1785–1796, Jul. 2014.

[23] D. E. Olivares, C. A. Cañizares, and M. Kazerani, "A centralized energy management system for isolated microgrids," *IEEE Trans. Smart Grid*, vol. 5, no. 4, pp. 1864–1875, Jul. 2014.

[24] Q. Jiang, M. Xue, and G. Geng, "Energy management of microgrid in grid-connected and stand-alone modes," *IEEE Trans. Power Syst.*, vol. 28, no. 3, pp. 3380–3389, Aug. 2013.

[25] R. V. A. Neves, R. Q. Machado, V. A. Oliveira, X. Wang, and F. Blaabjerg, "Multitask fuzzy secondary controller for AC microgrid operating in stand-alone and grid-tied mode," *IEEE Trans. Smart Grid*, vol. 10, no. 5, pp. 5640–5649, Sep. 2019.

[26] A. Zeh, M. Müller, M. Naumann, H. C. Hesse, A. Jossen, and R. Witzmann, "Fundamentals of using battery energy storage systems to provide primary control reserves in Germany," *Batteries*, vol. 2, no. 3, p. 29, 2016.

[27] K. Uddin, R. Gough, J. Radcliffe, J. Marco, and P. Jennings, "Techno-economic analysis of the viability of residential photovoltaic systems using lithium-ion batteries for energy storage in the United Kingdom," *Appl. Energy*, vol. 206, pp. 12–21, Nov. 2017.

[28] C. Ju, P. Wang, L. Goel, and Y. Xu, "A two-layer energy management system for microgrids with hybrid energy storage considering degradation costs," *IEEE Trans. Smart Grid*, vol. 9, no. 6, pp. 6047–6057, Nov. 2018.

[29] X. Ruan, X. Wang, D. Pan, W. Li, and C. Bao, *Control Techniques for LCL-Type Grid-Connected Inverters*. Beijing, China: Springer, 2018.

[30] P. Rodriguez, A. Luna, I. Candela, R. Mujal, R. Teodorescu, and F. Blaabjerg, "Multiresonant frequency-locked loop for grid synchronization of power converters under distorted grid conditions," *IEEE Trans. Ind. Electron.*, vol. 58, no. 1, pp. 127–138, Jan. 2010.

[31] A. G. Yepes, F. D. Freijedo, J. Doval-Gandoy, Ó. López, J. Malvar, and P. Fernandez-Comesaña, "Effects of discretization methods on the performance of resonant controllers," *IEEE Trans. Power Electron.*, vol. 25, no. 7, pp. 1692–1712, Jul. 2010.

[32] J. Nocedal and S. Wright, *Numerical Optimization* (Springer Series in Operations Research and Financial Engineering). New York, NY, USA: Springer, 2006.

ELIAN J. AGNOLETTO was born in Marcelino Ramos, Brazil. He received the B.S. degree in electrical engineering from the Universidade Federal de Mato Grosso, in 2012, and the M.S. degree in electrical engineering from the Universidade de São Paulo, in 2015, where he is currently pursuing the Ph.D. degree. His research interests include renewable power systems, energy management systems applied to distributed generation in microgrids, and power quality issues of electrical systems.

DANIEL SILVA DE CASTRO received the B.Eng. degree in electrical engineering from the Federal University of Ouro Preto, João Monlevade campus, MG, Brazil, in 2018. He is currently pursuing the M.Sc. degree in electrical engineering with the University of São Paulo. His research interests include analysis and design of new power converters, applied control in power electronic devices and electric machines, microgrids, and real-time simulation of dynamic systems.

RODOLPHO V. A. NEVES received the B.S. degree in electrical engineering from the Universidade Federal de Viçosa, Brazil, in 2011, and the M.Sc. and Ph.D. degrees in electrical engineering from the Universidade de São Paulo, São Carlos, Brazil, in 2013 and 2018, respectively. From 2015 to 2016, he was a Visiting Researcher with Aalborg University, Denmark. He is currently an Assistant Professor with the Department of Electrical Engineering, Universidade Federal de Viçosa. His research interests include control systems and microgrid management.

RICARDO QUADROS MACHADO was born in Santa Maria, Brazil. He received the B.S. degree from the University of Santa Maria, Santa Maria, in 1997, and the M.S. and Ph.D. degrees in electrical engineering from the University of Campinas, Campinas, Brazil, in 2000 and 2005, respectively. From 2002 to 2003, he was a Visiting Researcher with the University of Padova, Padova, Italy, and from 2005 to 2007, he was a Postdoctorate with the Federal University of Santa Maria, Santa Maria. From 2013 to 2014, he was a Visiting Professor with the University of Toronto, Toronto, Canada. From 2007 to 2018, he was an Assistant Professor with the University of São Paulo, São Carlos, Brazil, where he is currently an Associate Professor. His main research interests include processing of energy in dc/dc and dc/ac converters, digital control of power converters, distributed generation systems, smart grids, and control of renewable energy sources.

VILMA A. OLIVEIRA received the B.Eng. degree in electronics from the Universidade do Estado do Rio de Janeiro, Brazil, in 1976, the M.Sc. degree in electrical engineering from the Universidade Federal do Rio de Janeiro, in 1980, and the Ph.D. degree in electrical engineering from the University of Southampton, U.K., in 1989. In 1990, she joined the Electrical and Computing Engineering Department, Universidade de São Paulo, São Carlos, Brazil, where she is currently a Full Professor. Her research interests include fuzzy control and control design and its applications.

• • •